ELSEVIER

Surface Science 415 (1998) L976–L982

surface science

Surface Science Letters

High-resolution structural study of zinc ion incorporation at the calcite cleavage surface

L. Cheng [a,b], N.C. Sturchio [b,*], J.C. Woicik [c], K.M. Kemner [b], P.F. Lyman [a], M.J. Bedzyk [a,d]

[a] *Department of Materials Science and Engineering, and Materials Research Center, Northwestern University, Evanston, IL 60208, USA*
[b] *Environmental Research Division, Argonne National Laboratory, Argonne, IL 60439, USA*
[c] *National Institute of Standards and Technology, Gaithersburg, MD 20899, USA*
[d] *Materials Science Division, Argonne National Laboratory, Argonne, IL 60439, USA*

Received 3 April 1998; accepted for publication 1 July 1998

Abstract

The atomic-scale structure of Zn^{2+} incorporated at the $CaCO_3$ $(10\bar{1}4)$ surface by adsorption from solution was determined by X-ray standing wave triangulation and surface extended X-ray absorption fine structure spectroscopy. At low coverage (approximately 0.1 ML), Zn^{2+} substitutes for Ca^{2+} in the surface layer. Structural relaxation of the adjacent in-plane CO_3^{2-} ions in the host surface is shown by the reduced nearest-neighbor distance of Zn–O relative to Ca–O. Relaxation of the Zn^{2+} ion in the out-of-plane direction is shown by the displacement of its lattice position from the ideal Ca^{2+} position. These relaxations, resulting in a local lattice buckling feature at the Zn^{2+} adsorption site, can be fully explained as the combined effect of the electrostatic relaxation of the nearest-neighbor anions in response to the smaller size of Zn^{2+}, and the bonding asymmetry due to surface truncation.

Keywords: Adsorption; Calcite; Surface extended X-ray absorption fine structure (SEXAFS); Surface structure; X-ray standing waves (XSW); Zinc

The buckled lattice structure observed in a mixed ionic crystal [1,2] reveals the cooperative characteristics of ionic bonding. Despite the differences in size of the mixing ions, the crystal nonetheless maintains an average long-range lattice order. The geometric flexibility for bonding among ions of different sizes is attributed to the long-range nature of the electrostatic potential, which is attractive among nearest neighbors; the preservation of lattice ordering, on the other hand, is ensured by the cut-off to this attractive force imposed by the strong short-range repulsive potential of the electron shells. This type of balance between the attractive and the repulsive forces among nearest-neighbor ions is presumably also the primary mechanism that determines the structure of an impurity ion incorporated at the surface of an ionic crystal, creating a localized lattice buckling feature at the impurity adsorption site analogous to those in the bulk. Unlike the bulk lattice, however, the surface impurity is not fully coordinated due to the truncation of the crystal; this may render further structural ordering at the impurity site.

* Corresponding author. Fax: +1 630 252 7415; e-mail: sturchio@anl.gov

0039-6028/98/$ – see front matter
PII: S0039-6028(98)00545-7

A precise knowledge of the local lattice structure of a surface impurity ion is a critical factor in one's ability to accurately assess the properties of the impurity-doped surface, that is, whether the surface preserves sufficient ordering for further epitaxial growth into a potentially macroscopic solid solution phase, or the impurity doping may passivate or inactivate the surface. These fundamental issues have practical significance in many applied systems. Although there have been numerous studies on ionic surfaces, most have focused only on adsorption at binary surfaces such as alkali and alkaline–earth halides and metal oxides, in the on-top or hollow geometries by isolated bonding [3]. Little attention has been paid to the structure of a substitutional impurity ion incorporated in an ionic surface.

In this report, we present the results of a combined X-ray standing wave (XSW) triangulation and surface extended X-ray absorption fine structure (SEXAFS) study on the structure of an absorbed Zn^{2+} impurity ion on the $CaCO_3$ $(10\bar{1}4)$ surface. The combination of these two techniques allows us to obtain two complementary pieces of structural information at the atomic scale. From XSW triangulation, we obtain the lattice site of the adsorbate ion with respect to the substrate crystal, and from SEXAFS, we obtain the local relaxation of the host lattice at the adsorption site with respect to the impurity ion. The back-reflection XSW and SEXAFS techniques have previously been used together to study surface relaxation [4]; the present work is, to our knowledge, the first to be reported combining the conventional XSW triangulation and SEXAFS.

The calcite $(10\bar{1}4)$ surface used in these experiments is highly ordered. The unit cell parameters of this surface preserve their bulk values in aqueous environment and in vacuum, as revealed by atomic force microscopy [5,6] and low-energy electron diffraction studies [7], respectively. The out-of-plane relaxation of the surface is small at the high-symmetry lattice points according to X-ray scattering characterization [8]. The Zn^{2+} ion is isovalent to the host Ca^{2+} ion, but is substantially smaller in size (ionic radii: Zn^{2+}, $r=0.74$ Å; Ca^{2+}, $r=0.99$ Å). This difference in ionic size is expected to cause structural relaxation at the adsorption site.

Zn^{2+} ions were adsorbed on freshly-cleaved natural Iceland spar $(10\bar{1}4)$ surfaces from a dilute ($[Zn^{2+}]=0.63$ mM) aqueous solution. The solution contained an excess of ethylenediaminetetraacetic acid (EDTA) to ensure that no separate Zn solid phase became saturated. After adsorption in solution, excess solution over the sample surface was removed by a jet of dry nitrogen gas without allowing precipitation. The samples were maintained in a helium environment during X-ray measurements. We use the term "adsorption" in a general sense without specifically suggesting the nature of chemical bonding or the geometry of the "adsorbate"; these are to be resolved by the analysis of the experimental results.

Both the XSW and the SEXAFS experiments were carried out at beamline X15A at the National Synchrotron Light Source. The Bragg-diffraction XSW technique, which is reviewed in ref. [9], has previously been applied to studying adsorption of metal ions on calcite surface [10–12]. The XSW at the calcite crystal surface, which is generated by the interference between the incident and Bragg-diffracted X-ray beams, is shifted inward in the $-[hkil]$ (or $-H$) direction by one-half of the d-spacing during the course of scanning through the $(hkil)$ reflection. In the present case, this produces a characteristic modulation in the normalized Zn Kα yield, which is described as

$$Y(\theta)=1+R(\theta)+2\sqrt{R(\theta)}f_H\cos[v(\theta)-2\pi P_H] \quad (1)$$

where $R(\theta)$ is reflectivity and $v(\theta)$ is the relative phase of the standing-wave field. The coherent position P_H is the average $\Delta d_H/d_H$ position of the adion, and the coherent fraction f_H and P_H are the amplitude and phase, respectively, of the H Fourier component of the normalized spatial distribution of the fluorescent adions. In practice, $Y(\theta)$ is measured, and f_H and P_H are obtained as best-fit parameters through Eq. (1).

The XSW experiments were performed using the $(10\bar{1}4)$ normal lattice planes, and the (0006) and $(02\bar{2}4)$ off-normal lattice planes. The incident X-ray beam was monochromated to 11.0 keV with a double-crystal monochromator, using Si(111) for the calcite $(10\bar{1}4)$ and (0006) reflections, and

Si(022) for the $(02\bar{2}4)$ reflection. In each setting, the first of the two Si monochromator crystals had a suitable surface miscut to optimize beam collimation. The sample was placed on a four-circle diffractometer. The reflectivity and fluorescence signals were simultaneously recorded, respectively, with a Si photodiode and an energy-dispersive Si(Li) solid-state detector.

The principles and experimental techniques of SEXAFS are reviewed in Ref. [13]. The SEXAFS measurement presented here was taken on the same sample on which XSW measurements had been made, using X-rays monochromated with a symmetric Si(111) double crystal monochromator over the Zn *K*-edge, in an energy range of 9.6–10.1 keV. The beam was incident on the sample surface at a glancing angle of approximately 10°, so that the σ-polarized *E*-field preferentially sampled bonding that was within the $(10\bar{1}4)$ lattice plane. Data were collected in the fluorescence mode with the Si(Li) detector by monitoring the Zn Kα fluorescence. A thin Ho_2O_3 foil was used to reduce elastically scattered signals. The fluorescence emission angle from the sample surface was controlled by a low-angle slit placed between the sample and the detector to enhance surface sensitivity.

The experimentally measured reflectivity $R(\theta)$ and Zn^{2+} fluorescence yield $Y(\theta)$ with respect to the normal $(10\bar{1}4)$, and the off-normal (0006) and $(02\bar{2}4)$ lattice planes for a typical sample are presented in Fig. 1, along with the best-fit curves based on Eq. (1) to these data. The corresponding coherent positions P_H and coherent fractions f_H obtained from these fits are given in the figure. This sample had a total Zn^{2+} adsorbate coverage of $\Theta_T = 0.10 \pm 0.02$ ML, as measured against a calibrated Ga-implanted silicon standard crystal; the coherent coverage was therefore $\Theta_C = f_{10\bar{1}4} \times \Theta_T = 0.09 \pm 0.02$ ML. The 0.02 ML uncertainty in coverage was shown by a separate full XSW scan on a control calcite substrate to be due to background signals not originating from the sample surface or substrate. Independently, chemical analysis of the calcite substrate showed that it contained less than 3 ppm of Zn as impurities. For the Zn^{2+}-adsorbed samples, although the Zn fluorescence signal in principle could have

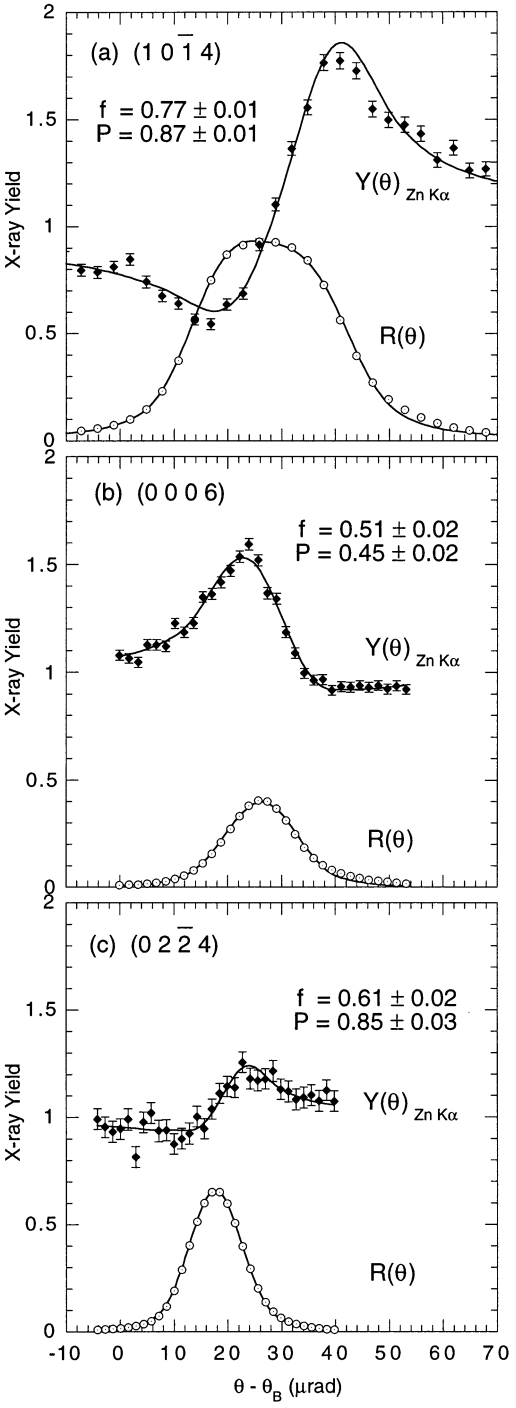

Fig. 1. X-ray standing wave triangulation results. X-ray reflectivity $R(\theta)$ and Zn Kα fluorescence yield $Y(\theta)$ measured for the calcite (a) $(10\bar{1}4)$, (b) (0006) and (c) $(02\bar{2}4)$ Bragg reflections. The solid lines are the best χ^2 fits to the data; the best-fit results and uncertainties are shown in the figure.

originated from anywhere within the 14.6 μm extinction depth of the Zn Kα X-ray, careful XSW experiments on the $(10\bar{1}4)$ reflection with fluorescence slit set at various take-off angles (from less than 1 to a few degrees) from the surface gave identical results in P_H. This indicates that the Zn signal was from the surface. Furthermore, the best fits for $Y(\theta)$ were obtained with the assumption that the Zn signals were from the surface. The XSW measurements were replicated on six other adsorption surfaces prepared with the same method, but with different adsorption time periods, ranging from 4 to 20 min. The P_H values for all reacted surfaces remained unchanged within the range of experimental uncertainty; the average coherent position for the $(10\bar{1}4)$ reflection over all samples is 0.87, with a standard deviation of 0.008. The corresponding average coherent fraction over these samples is 0.61, with a standard deviation of 0.13. The average total Zn coverage over all samples is 0.13 ML, with a standard deviation of 0.04 ML. These data suggest that the adsorption site is constant, while the coherent fraction fluctuates slightly due to variations in sample preparation. The rate of adsorption was apparently fast relative to the shortest solution exposure time. The fraction of Zn that is not coherent could represent disordered, hydrated Zn ions that are physisorbed to the surface, or Zn associated with adventitious material. A comparable study of Pb adsorption on calcite showed no difference between P_H values measured in situ and those measured after removing the solution from the surface by the procedure used in this study [11].

SEXAFS data analysis was performed using the MacXAFS software package [14] according to standard procedures [15]. After background subtraction and conversion to k-space, the k^2-weighted experimental EXAFS $\chi(k)$ function, shown in Fig. 2a, displays a dominant first-shell feature that is of the same frequency as the first-shell component in the $ZnCO_3$ standard compound, shown in Fig. 2b. The $\chi(k)k^2$ function was Fourier transformed into R-space over the range $k = 2.81$–10.48 Å^{-1}, with modified Hanning windows of 0.40 Å^{-1}, to reduce truncation ripple. The first-shell contribution of the Fourier-transformed data from both samples (Zn on calcite, and

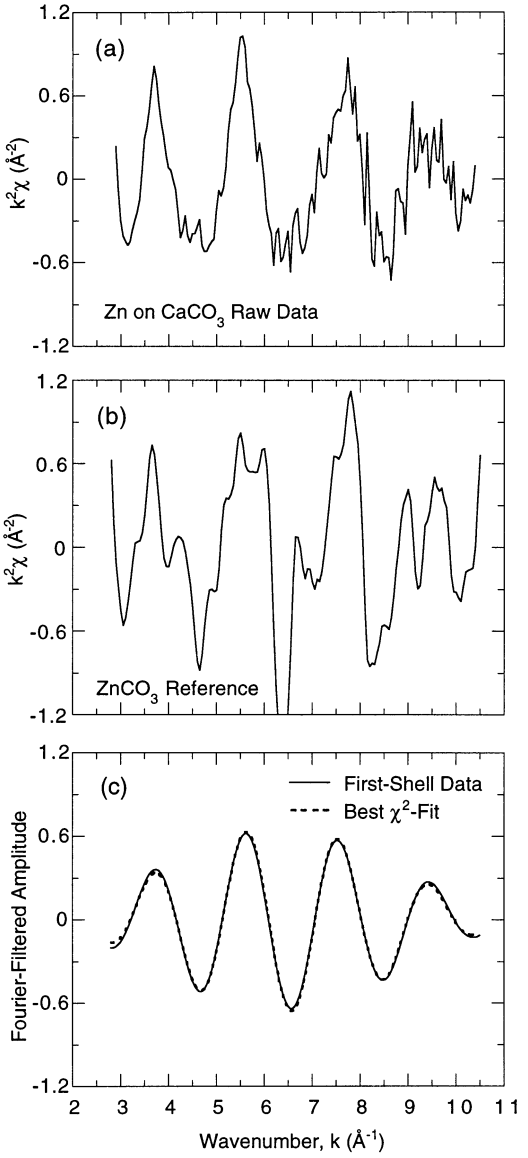

Fig. 2. The $\chi(k)k^2$ Zn K photoelectron experimental EXAFS spectra for (a) Zn on $CaCO_3$ sample, (b) $ZnCO_3$ standard, and (c) the Fourier-filtered Zn–O first-shell component of the Zn on $CaCO_3$ data (solid line). Also plotted in (c) is the best fit to the filtered first-shell data (dashed line).

$ZnCO_3$) was Fourier filtered ($R = 1.09$–2.16 Å, and 0.202 Å Hanning windows). The Fourier-filtered data from the Zn-on-calcite sample are shown as a solid line in Fig. 2c. This data was fit in phase $\phi(k)$ and amplitude $|f(k)|$ with respect to that for

the $ZnCO_3$ standard, according to the equation

$$\chi(k) = N|f(k)| \sin[2kR + \phi(k)] \exp(-2k^2\sigma^2). \quad (2)$$

The best fitting parameters are obtained by minimizing the normalized χ^2 value. This value is defined to be the difference in phase and amplitude of the filtered data of the experimental and computer-generated data. For the transform range (2.81–10.48 $Å^{-1}$) and Fourier filtering range (1.09–2.16 Å) used in this analysis, the maximum number of fit parameters allowed to vary at one time is more than five [16]. In addition to an energy shift variable (ΔE), three parameters were allowed to vary while determining the best fit to the data: the Zn–O radial distance (R), the coordination number (N), and the mean-square relative displacements due to static distribution and thermal vibration (σ^2). The best-fit values for these parameters are $\Delta E = 0.65$ V, $R = 2.11 \pm 0.01$ Å, $N = 3.81 \pm 1$ and $\Delta\sigma^2 = 0.0013 \pm 0.001$ Å^2. The coordination number value quoted here has been normalized to account for a maximum allowed in-plane Zn–O coordination number of 4. The $\Delta\sigma^2$ value represents a difference relative to the $ZnCO_3$ standard. Additionally, the errors quoted in the best-fit values for R and $\Delta\sigma^2$ represent an increase in the χ^2 value from approximately 0.5 to 2 as each fitting variable was stepped across its best-fit value while allowing the remaining fit variables to float. The error quoted for N is estimated [15]. The ΔE value never varied by more than 0.15 V from the best-fit value of 0.65 V. The best fit to the Fourier-filtered data is shown as a dash line in Fig. 2c.

The two-dimensional primitive unit cell for the $(10\bar{1}4)$ lattice plane in calcite contains two $CaCO_3$ molecules. In the bulk lattice, each of the two central Ca^{2+} ions is octahedrally coordinated to six nearest-neighbor oxygen atoms in the six adjacent CO_3 groups. Four of six O atoms are on the same $(10\bar{1}4)$ lattice plane as the central Ca^{2+} ion, and the remaining two are in the adjacent $(10\bar{1}4)$ planes. As the $(10\bar{1}4)$ surface is created, the O atom above the surface plane is removed.

In the following we present a structural interpretation of the XSW and SEXAFS results. First, by comparing the Zn coherent positions to those for the Ca and considering the number of nearest-neighbor coordinated O atoms, we establish that Zn^{2+} substitutes for Ca^{2+} on the surface lattice plane. We then describe the local in-plane relaxation of the surrounding O atoms by considering the first nearest-neighbor Zn–O distance. Finally, from the Zn coherent positions measured with respect to the three non-colinear lattice planes, we determine the exact lattice sites of the Zn^{2+} adsorbate ions. A quantitative structural model of the Zn^{2+} ions incorporated in the calcite $(10\bar{1}4)$ surface that is consistent with the experimental observations is then presented.

The P_H values for each of the two ideal Ca sites with respect to the $(10\bar{1}4)$, (0006), and $(02\bar{2}4)$ lattice planes are 1, 0.5, and 1, respectively. The corresponding measured P_H values for Zn, of 0.87, 0.45, and 0.85, indicate that the Zn^{2+} ion is located within the oxygen-cornered cation octahedron, but slightly displaced from its center where the Ca^{2+} would be located. This leads to the conclusion that Zn^{2+} substitutes for Ca^{2+} at its high-symmetry sites. This is, to our knowledge, the first direct structural evidence that Zn^{2+} substitutes for Ca^{2+} upon adsorption on calcite surface from solution; previous assertions of this generally accepted notion have been based on indirect inference from solution ion concentration changes observed from before to after adsorption, e.g. Ref. [17]. To resolve whether the Zn^{2+} ion is adsorbed in an on-top geometry or incorporated in the surface layer requires the Zn–O nearest-neighbor coordination information. The coordination number N for a surface cation site is expected to be approximately 4, and the measured Zn–O coordination number of 3.81 ± 1 indicates that Zn^{2+} is incorporated in the surface layer. If the Zn^{2+} adsorbate were located above the surface, or occurred for example as an amorphous hydroxide phase, it would most likely have different values of R and/or N than those measured.

Since the Zn^{2+} ion is substantially smaller than the Ca^{2+} ion, inward relaxation of its nearest-neighbor CO_3^{2-} groups on the surface may occur. This was indeed observed in the Zn–O nearest-neighbor distance of 2.11 ± 0.01 Å. Since the Ca–O nearest-neighbor distance in the ideal calcite lattice is 2.36 Å, an inward relaxation of 0.25 Å is observed. Note that this measured Zn–O nearest-neighbor distance is within uncertainty equal to

the Zn–O distance in $ZnCO_3$, of 2.111 Å [18]. That is, the nearest-neighbor O atom bound to the CO_3^{2-} group relaxed fully so that Zn and O are in "contact". This hints that the attractive electrostatic interaction of the substituting cation with its nearest-neighbors is the driving force of this local relaxation. In other words, given its identical valence to the host cation, the local in-plane structure of an adsorbate cation is determined solely by its ionic size.

The relaxation of the Zn^{2+} ion in the out-of-plane direction reflects the effect of surface truncation. The dominance of the nearest-neighbor electrostatic interaction in the in-plane structure considered above suggests that the out-of-plane relaxation may be along the Zn–O direction as well (where O specifies the coordinating oxygen atoms in the second layer). We may consider a hypothetical surface lattice model for the two sites of the surface Zn^{2+} ions, assuming they relax along the out-of-plane nearest-neighbor Zn–O direction by such a distance that their positions projected in the $(10\bar{1}4)$ lattice normal agree with that measured by XSW. We then verify the validity of this model by checking its quantitative consistency in the Zn^{2+} positions with respect to the off-normal (0006) and $(02\bar{2}4)$ planes with that from the XSW measurements. The model is shown in Fig. 3. The quantitative positions h_H of the Zn^{2+} ions above the lattice plane H at the two generally non-equivalent cation sites in a surface unit cell derived from this model are listed in Table 1, and compared to that from the XSW measurements, with the relation $h_H = d_H \times P_H$. Note that the two Zn sites are inequivalent with respect to the $(02\bar{2}4)$ planes, but equivalent with respect to the $(10\bar{1}4)$ and the (0006) planes. The agreement between the values from the model and from the XSW experiments indicates that the model is valid within uncertainties. Furthermore, if we assume the oxygen atoms coordinated to the Zn^{2+} adsorbate ion from the second-layer CO_3^{2-} are bulk-like in position, the Zn–O nearest-neighbor distance in the out-of-plane direction is deduced to be 1.95 Å from the model. This distance is comparable to the Zn–O bond distance found in more tightly bound binary compounds, e.g. ZnO. The shorter Zn–O bond distance in the out-of-plane direction compared to that in-plane is not unexpected, and is obviously best explained by the bonding asymmetry at the surface.

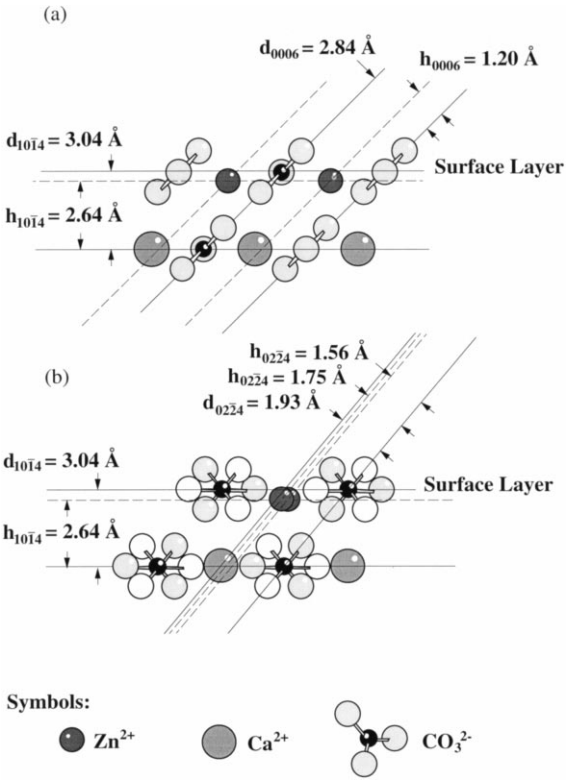

Fig. 3. A model describing the lattice sites of the Zn^{2+} ions (showing the local relaxation of the CO_3^{2-} ions) incorporated in the $CaCO_3$ $(10\bar{1}4)$ surface. The Zn^{2+} lattice sites in the model are constructed assuming that Zn^{2+} ions are in the surface monolayer, and their out-of-plane relaxation is along the direction of the nearest-neighbor Zn–O (O in the second-layer) bond. (a) An edge-on view of the adsorption surface containing the $(10\bar{1}4)$ and (0006) planes. (b) An edge-on view containing the $(10\bar{1}4)$ and $(02\bar{2}4)$ planes.

It is particularly noteworthy that the extent of the in-plane relaxation of the nearest-neighbor O atoms towards Zn^{2+} at the calcite surface is equivalent within uncertainty to that occurring at a Zn^{2+} impurity site in bulk calcite, where the Zn–O distance is 2.12 ± 0.02 Å [19]. The significance of this comparison between the surface and the bulk impurity structure is that it implies that the calcite $(10\bar{1}4)$ surface, in addition to being structurally bulk-like, must also possess bulk-like parameters

Table 1
Lattice position h_H of the Zn^{2+} ion above the lattice plane H from the XSW measurements and according to the structural model described in the text. Note that for $H=(02\bar{2}4)$, where the two non-equivalent Zn^{2+} sites project different h_H positions, the XSW measured position is the average of the two projected positions. The uncertainties in the XSW measured values are estimated from consideration of the uncertainties in P_H from the best χ^2 fits (listed in Fig. 1) and, in the case for $H=(10\bar{1}4)$, the statistical distribution in P_H from all samples examined (see text); these uncertainties correspond to 1%, 5% and 3% of the d-spacing for the $(10\bar{1}4)$, (0006) and $(02\bar{2}4)$ reflections, respectively

H	d_H (Å)	h_H (XSW measured)	h_H (model)	
			Site 1	Site 2
$(10\bar{1}4)$	3.04	2.64 ± 0.03	2.64 ± 0.03	2.64 ± 0.03
(0006)	2.84	1.28 ± 0.14	1.20 ± 0.04	1.20 ± 0.04
$(02\bar{2}4)$	1.93	1.64 ± 0.06	1.75 ± 0.05	1.56 ± 0.05

in its interaction potentials (i.e. the Madelung and Born-type potentials), at least at the cation sites.

In summary, using X-ray standing wave triangulation and surface extended X-ray fine structure spectroscopy, we determined in high resolution the adsorption structure of Zn^{2+} incorporated at the calcite cleavage surface from an aqueous solution. The adsorption is substitutional, in the surface layer. The nearest-neighbor O atoms at the adsorption site relax inward, because of the smaller ionic size of Zn^{2+}, to such an extent that the Zn–O distance is equivalent to that found in the isomorphous $ZnCO_3$ crystal structure. The slight displacement of the Zn^{2+} adsorbate from the center of the Ca^{2+} octahedron is explained by the surface truncation-induced asymmetry on the bulk relaxation in the out-of-plane direction.

Acknowledgements

This research was supported by the Geosciences and Materials Science Research Programs of the Office of Basic Energy Sciences, US Department of Energy, under Contract W-31-109-Eng-38 to Argonne National Laboratory, by DOE Contract DE-AC02-76CH00016 to the National Synchrotron Light Source at Brookhaven National Laboratory, and by the National Science Foundation under Contract DMR-9632472 to the Materials Research Center at Northwestern University.

References

[1] J.B. Boyce, J.C. Mikkelsen, Phys. Rev. B 31 (1985) 6903.
[2] A. Frenkel, E.A. Stern, A. Voronel, M. Qian, M. Newville, Phys. Rev. Lett. 71 (1993) 3485.
[3] H.-J. Freund, E. Umbach (Eds.), Adsorption on Ordered Surface of Ionic Solids and Thin Films, Springer, Heidelberg, 1993.
[4] J.C. Woicik, T. Kendelewicz, A. Herrera-Gomez, K.E. Miyano, P.L. Cowan, C.E. Bouldin, P. Pianetta, W.E. Spicer, Phys. Rev. Lett. 71 (1993) 1204.
[5] F. Ohnesorge, G. Binnig, Science 260 (1993) 1451.
[6] Y. Liang, A.S. Lea, D.R. Baer, M.H. Engelhard, Surf. Sci. 351 (1996) 172.
[7] S.L. Stipp, H.F. Hochella, Geochim. Cosmochim. Acta 55 (1991) 1723.
[8] R.P. Chiarello, N.C. Sturchio, Geochim. Cosmochim. Acta 59 (1995) 4557.
[9] J. Zegenhagen, Surf. Sci. Rep. 18 (1993) 199.
[10] Y. Qian, N.C. Sturchio, R.P. Chiarello, P.F. Lyman, T.-L. Lee, M.J. Bedzyk, Science 265 (1994) 1555.
[11] N.C. Sturchio, R.P. Chiarello, L. Cheng, P.F. Lyman, M.J. Bedzyk, Y. Qian, H. You, D. Yee, P. Geissbuhler, L.B. Sorensen, Y. Liang, D. Baer, Geochim. Cosmochim. Acta 61 (1997) 251.
[12] L. Cheng, P.F. Lyman, N.C. Sturchio, M.J. Bedzyk, Surf. Sci. 382 (1997) L690.
[13] J. Stohr, in: D.C. Koningsberger, R. Prins (Eds.), X-ray Absorption. Principles, Applications, Techniques of EXAFS, SEXAFS and XANES, Wiley, New York, 1988.
[14] C. Bouldin, L. Furenlid, T. Elam, Physica B 208/209 (1995) 190.
[15] D.E. Sayers, B.A. Bunker, in: D.C. Koningsberger, R. Prins (Eds.), X-ray Absorption. Principles, Applications, Techniques of EXAFS, SEXAFS and XANES, Wiley, New York, 1988.
[16] S.S. Hasnain (Ed.), X-ray Absorption Fine Structure, Ellis Horwood, New York, 1991.
[17] J.M. Zachara, J.A. Kittrick, J.B. Harsh, Geochim. Cosmochim. Acta 52 (1988) 2281.
[18] H. Effenberger, K. Mereiter, J. Zemann, Z. Kristallogr. 156 (1981) 233.
[19] G.M. Lamble, R.J. Reeder, P.A. Northrup, J. Phys. (Fr.) IV 7 (1997) C793.